Properties of Porous Tungsten for Surface Ionizers

ROBERT G. WILSON,* PETER SCHWARZKOPF,† GORDON D. SEELE,‡ AND J. F. HON§
North American Aviation, Inc., Canoga Park, Calif.

The structural properties of porous tungsten ionizers sintered from powders of grain sizes 0.1, 0.9, 5, 8, 12 to 18, and 44 to 74 μ were investigated by gas-flow and metallographic techniques. The quantitative influence of porosity and further sintering on the structural characteristics are presented. The experimental results indicate that powders of less than 1- or 2-μ diam cannot be used to fabricate satisfactory sintered porous ionizers unless significant advances are made in the techniques of powder metallurgy and sintering. Because the ionizer permeability and specific periphery increase with increasing porosity at a given powder size, a high ionizer porosity at any given powder size (pore diameter) is expected to be desirable for electrical propulsion applications. The apparent perveance of all of the ionizers was observed to increase slightly with increasing ion-current density and to decrease with increasing ionizer powder size. The operating characteristics of the 0.9-μ ionizer deteriorated severely with operating time at operating temperatures above 1100°C. The ionization efficiency decreases with increasing ion-current density at constant temperature (with some exceptions), and the ionization efficiency decreases with increasing ion-current density more rapidly as the ionizer powder size (pore size) increases. The maximum ionization efficiency was observed to occur at temperatures above the critical temperature. If high values of both ionization efficiency and ion-current density are simultaneously desirable, then this work leads to the conclusion that as small an initial ionizer powder size as possible (within the lower limit imposed by sintering changes, which is, at present, about 2 μ) be combined with higher ionizer temperature and high ionizer porosity.

Nomenclature

A = area
D = mean grain diameter
E = applied electric field strength
F = conductance
H = surface pore density of ionizer
J_+ = ion-current density
L = thickness of porous medium
L_c = mean length of pore (channel) in porous medium ($L_c > L$)
M = molecular weight
N_a = Avogadro's number
P = perveance; pressure
P_0 = pressure of space or vacuum (on downstream side of porous medium)
P_V = vapor pressure
P^* = apparent perveance
P_s = specific periphery
S = mean interpore spacing
S_V = specific surface
T = temperature
V = applied potential
V_i = ionization potential
V_m = activation energy for surface migration
d = mean pore diameter
e = electron charge or electron designation
f = fractional area
k = Boltzmann's constant
k_p = permeability
n_0 = neutral particle flux
n_+ = ion flux
n_T = total particle flux
v = flow velocity
x = distance
α = adsorption coefficient; ionization coefficient
β = surface ionization efficiency
δ = average distance between adsorption sites
η = viscosity
$\eta_v(T)$ = viscosity of vapor phase of transport substance
$\eta_c(T)$ = viscosity of condensed phase of transport substance
θ = surface coverage
λ = desorption energy
λ_+ = ion desorption energy
$\rho_c(T)$ = density of condensed phase of transport substance
$\sigma(1)$ = monolayer surface concentration
ψ = energy associated with electric field
ω = vibration frequency

Subscripts

c = critical
k = of kth type patch

Presented as Preprint 63-017 at the AIAA Electric Propulsion Conference, Colorado Springs, Colo., March 11–13, 1963; revision received July 31, 1964. This work was performed at the now nonexistent Electrical Propulsion Section of Rocketdyne.

* Research Specialist; now Member Technical Staff, Hughes Research Laboratories, Malibu, Calif. Member AIAA.

† Research Specialist, Materials Research Section, Rocketdyne Division. Member AIAA.

‡ Physicist, Electrical Propulsion Section; now Research Engineer, Research Department, Rocketdyne Division.

§ Principal Scientist, Ion Engine Physics Unit, Electrical Propulsion Section; now Principal Scientist, Ion and Plasma Physics Unit, Research Department, Rocketdyne Division. Member AIAA.

1. Introduction

ONE concept of advanced space propulsion involves the application of the phenomenon of surface ionization. Ions of a propellant species characterized by a low ionization potential are created at the surface of a high work-function heated refractory surface from which they are extracted, accelerated, and focused into a directed thrust-producing ion beam by a strong electric field. The most widely applied concept for such devices utilized porous tungsten for the ionizing surface and cesium for the propellant. The propellant migrates through the porous ionizer and onto the heated surface where the electric field is applied. The surface must be heated to provide thermal energy for desorption of the propellant ions. A high temperature, which increases with increasing propellant arrival flux, is required to maintain a surface coverage low enough that the composite propellant-ionizer work function is sufficiently greater than the propellant ionization potential, thereby resulting in a high propellant ionization efficiency.

Various properties of sintered porous tungsten used for surface ionization of cesium in ion-propulsion devices have been studied by a number of authors.[1-13] No systematic study of the influence of the initial grain size of the tungsten powder on the ionizing properties of the sintered ionizers has been reported. This communication reports the results of an investigation of the physical and metallurgical properties of sintered tungsten ionizers made by means of gas-flow and metallographic techniques. A subsequent experimental study of the sintered porous structures as cesium ionizers was performed. Two of the experimental conditions under which these measurements were made, the vacuum conditions and the ion-accelerating geometry, fall short of the most desirable conditions for testing cesium ion-propulsion devices. However, the results do show some trends related to grain size, and they may also be of interest in other applications. The pressure at which the measurements were performed was not low enough to guarantee uncontaminated surface conditions. The influence of any surface contamination is unknown. The electrode geometry was not designed to simulate actual ion-thrustor geometries, and the perveance measurements apply only to the simple geometry used rather than to an especially designed ion-gun geometry.

2. Physical and Metallurgical Properties of the Porous Tungsten Ionizers

The porous tungsten ionizers used in this study were 0.030 in. thick and 0.25 in. in diameter. They were fabricated by the compaction of tungsten powders of single-sized grains, or of grains in the size ranges of 0.1, 0.9, 5, 8, 12 to 18, and 44 to 74 μ. Compaction was followed by sintering to bulk densities of from 60 to 80% of the theoretical density (19.3 g/cm^3) as listed in Table 1. Examples of initial sintering conditions are: 2350°C for 2 hr for the 5- and 8-μ specimens, and 1300°C for 15 min for the 0.9-μ ionizer.

Further long-term sintering experiments with the 0.1-, 0.9-, 5-, and 8-μ samples (100 hr at 800°C, followed by 100 hr at 1200°C, followed by 100 hr at 1600°C) showed[3] a decrease in ionizer porosity in all three cases, following the 1600°C test, but little or none following the 800 and 1200°C runs for the 5- and 8-μ specimens. The sintering data for the 0.9-μ ionizer at 1200°C were inconclusive but later flow-rate measurements with cesium proved that a significant decrease in permeability (and porosity) occurred with operating time in the range of 1200 to 1300°C. The 0.1-μ specimen exhibited cracks and signs of pore shrinkage even after 100 hr at 800°C, whereas the 1200° and 1600°C conditions showed increasing tendencies for grain coalescence and disappearance of the smaller pores, resulting in an increase in the mean pore size and decreases in the porosity and permeability. After the 1600°C run, the surface of the 0.1-μ specimen was so ruptured and so few pores remained that its use as an ionizer was impossible. Experimental test data showed that, for the 0.9-μ ionizer, significant decreases occurred in both the neutral cesium flowrate through the ionizer and in the perveance, or ion-current producing capabilities, with operating time and temperature. This indicated that the permeability and number of active pores decreased for the testing temperatures and times.

This information for the 0.1- and 0.9-μ ionizers clearly indicates that powders of less than 1 or 2 μ in diameter cannot be used to fabricate satisfactory sintered porous tungsten ionizers unless significant advances are made in the techniques of powder metallurgy and sintering.

The pores formed by the voids between neighboring tungsten particles act as capillary channels through the body of the ionizer. These channels are not straight, may change irregularly in cross section along their length, and may be distributed in a nonuniform manner throughout the bulk of the porous structure. Isolated, noninterconnecting porosity and dead-end channels are possible. The porous tungsten ionizers used in the surface ionization studies, and the compacts formed and sintered under identical conditions, were subjected to density measurements, gas-flow testing, and metallographic examination to determine a group of parameters for comparison of their porous structure.

From gas-flow measurements, the following parameters were determined: the conductance, the specific internal surface area per unit volume, the permeability, the mean grain diameter, the mean pore diameter, and the mean interpore spacing. The metallographic examinations yielded the statistical distributions of the interpore spacings, the grain sizes, and the pore sizes, from which the mean interpore spacings, the mean pore sizes, and the mean grain sizes were determined. A summary of these studies is presented here, together with Table 1, which tabulates the combined results.

Because the permeability, the measure of the ease with which a fluid flows through a porous medium under the influence of a pressure gradient, is not always defined in the same way, the definition, as used herein, and its relationship to the conductance are shown in the equation

$$k_p = \frac{\eta v}{dP/dx} = \frac{\eta dx}{AdP} F \qquad (1)$$

The units of permeability are cm^2.

Table 1 Summary of air-flow calculations and metallographic analyses of sintered porous tungsten ionizers[a]

Unsintered powder diam, μ quoted	% of theoretical density; density measurement	Mean pore diam (d), μ		Mean grain diam (D), μ		Mean interpore spacing (S), μ		Permeability (k), cm^2 air flow	Specific surface (Sv), cm^2/cm^3 (Knudsen air flow)	Specific periphery (P_S), μ/μ^2 3.6 d/S^2
		Air flow	Metallographic	(Poiseulle) air flow	Metallographic	Air flow	Metallographic			
0.1	This ionizer exhibited numerous cracks and no definite pore structure									
0.9	76	1.1	1.3	0.9	3.4	5.4	4.2	8.7×10^{-12}	9.6×10^5	0.13
5	80	...	2.8[b]	...	5.5[e]	...	12[e]	3×10^{-10}[e]	...	0.070
8	68	5.9[d]	6.0[d]	...	...	...	17[d]	2×10^{-9}[e]	...	0.062
12–18	68	16	9.7	13	23	27	27	2.1×10^{-8}	2.9×10^4	0.064
44–74	63	35	40	40	58	61	77	9.3×10^{-8}	8.3×10^4	0.027
8	60	6.6	6.4	3.9	8.8	28	17	7.2×10^{-9}	2.5×10^4	0.081
8[c]	70	5.9	6.0	5.0	10	32	17	3.7×10^{-9}	2.1×10^4	0.073
8[c]	80	6.2	6.6	8.3	14	42	19	2.3×10^{-9}	1.4×10^4	0.064
8[c]	90	4.8	5.4	19	16	35	17	1.2×10^{-9}	4.5×10^3	0.063

[a] The information presented for the sequence of 8-μ ionizers of varying density was obtained before the specimens were operated as cesium ionizers. For the varying grain-size sequence, the information was obtained after considerable use at elevated temperatures as cesium ionizers.
[b] From Ref. 1 or 2.
[c] Not studied with the neutral atom detector.
[d] Assumed from 8 (70 %) values.
[e] Determined from comparisons with cesium flow characteristics.

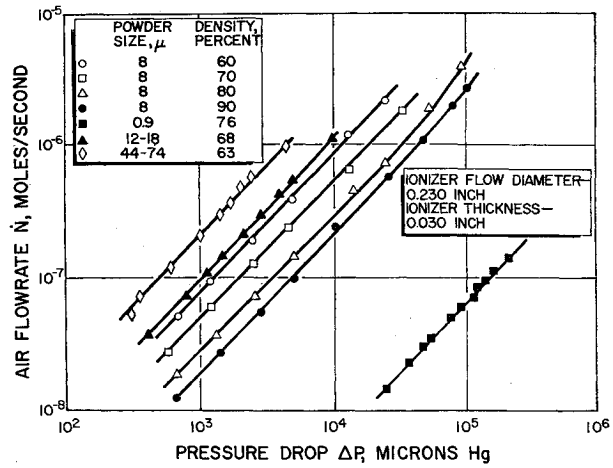

Fig. 1 Air flow rates vs pressure drop for porous tungsten ionizers.

The treatment of gas flow, due to Adzumi,[14] was used to calculate the mean pore size and pore density of the ionizers. Similar considerations were used to calculate the specific internal surface area of the porous microstructures according to the treatment of Deryagin[15] for molecular flow. A series-parallel capillary arrangement was assumed to exist in the porous ionizer. It has been shown experimentally[16] that the mean grain diameter is given by

$$D = 6/S_V \qquad (2)$$

where S_V is calculated from the permeability.

The ionizers were experimentally tested with dry air, hydrogen, and argon to obtain a range of viscosities and molecular weights. The measurements were made in the pressure range 5×10^{-5} to 760 mm Hg and at room temperature. The results of air flow as a function of pressure drop through the specimens are plotted in Fig. 1. The slopes of these log-log plots are unity, i.e., the equations are linear, which is characteristic of Knudsen molecular flow. A slight increase in slope at high values of ΔP for some specimens indicates a transition to Poiseulle viscous flow. From these and other data, plots of the conductance as a function of average pressure were drawn. From the resulting slopes and zero pressure intercepts, the various microstructural properties of the porous plugs were calculated. A summary of the results is presented in Table 1.

The problems posed by metallographic analyses of porous microstructures are twofold. First, for an analysis to be reliable, a large number (>600) of grains or pores must be measured on a representative metallographic section. Secondly, the pore and grain size measurements made on a two-dimensional cross section must be related to the actual volume distribution in the specimen.

The grain and pore size distributions were determined with a semiautomatic measuring and counting instrument, the Zeiss TGZ-3 Particle Size Analyzer. The ionizers were first infiltrated with a copper/2% nickel alloy. Photomicrographs were then made of polished representative sections of each ionizer. The magnifications were chosen for easy use with the Zeiss Particle Size Analyzer in that the minimum diameter measured was not less than 1 mm. The pore size distribution curves were plotted in cumulative and differential form, some of which are shown in Fig. 2. The mean pore size occurs at 50% on the cumulative curve.

For porous ionizers, the pore statistics may have a significant influence on the ionization efficiency and on the current-producing capabilities of the ionizer, i.e., upon the perveance of the system. Because ions can be produced and extracted efficiently from only a fraction of the total ionizer surface for a given set of conditions of cesium vapor pressure and surface temperature corresponding to that fraction of the surface for which $0 < \theta < \theta_c$, the size and surface density of the pores may affect the ion-current density. Because the cesium must migrate onto the ionizing surface over the pore edges, a high surface density of pore edge is desirable. A term is defined to serve as a relative measure of the amount of pore edge for various ionizers. This term, specific periphery P_s, is defined as the total pore periphery per unit area of ionizer surface, measured in reciprocal microns or centimeters, and is analogous to the specific surface of a porous ionizer, the total internal pore surface area per unit volume. An exact measure of P_s cannot easily be made because the details of the shapes of the individual pore openings and their surface distributions would need to be known. However, a significant relative value can be obtained by assuming that all of the pores are circles with a diameter equal to the mean pore diameter obtained from metallographic and gas-flow measurements, and that they are spaced uniformly in some geometrical array for which the mean interpore spacing can serve as a measure. Arbitrarily choosing a hexagonal close-packed pore distribution

$$P_s = (2\pi d/3^{1/2}S^2) = 3.6(d/S^2) \qquad (3)$$

Relative values of P_s have been calculated for the ionizers studied and are presented in the last column of Table 1.

A comparison of the metallographic and air flow results of pore and grain sizes is good in most cases. However, the values for the interpore spacing are in all cases lower for air flow than when observed directly by metallography. Two explanations are possible. First, the low values could be a shortcoming of the gas-flow method, attributable to the nature of the assumptions made concerning the capillary nature of the flow channels. Secondly, they could be an indication that not all of the pores observed by direct metallography are active, i.e., open. From the experimental results, it would seem that the effective free area to gas flow is much less than observed by metallography. This observation may be the result of a restriction of gas flow through a relatively small number of high-conductance channels formed by the bulk pore structure of the material. The previously mentioned decreases in permeability and porosity with operating time with cesium for the small grain sizes tend to support this theory. The values for mean grain diameter of the sintered ionizers obtained from gas-flow analysis were in agreement with the quoted initial particle sizes, but were smaller than the metallographic values (Table 1). This result is probably due to the technique used to measure initial grain size. Irregularly shaped particles, with surface areas larger than the same-diameter sphere, would register a smaller mean diameter than the average rounded metallo-

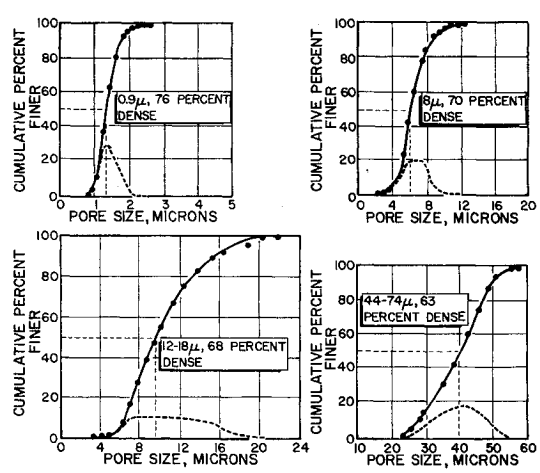

Fig. 2 Pore size distributions for the sintered tungsten ionizers (differential pore distribution shown by dashed curves).

graphic size. The permeability shown in Table 1 for the 0.9-μ ionizer is seen to be much lower than any others. It should be pointed out that the value reported for this ionizer was measured after the ionizer had been used in the neutral atom detector as a cesium ionizer at temperatures as high as 1300°C. As pointed out previously, the 0.1-μ ionizer permeability was essentially zero after sintering even at temperatures below or comparable to the critical temperature for ion production (~1150°K).

The data for the 8-μ porosity sequence (Table 1), obtained by variation of the sintering time, show the following: 1) the mean pore diameter and the mean interpore spacing remain relatively unchanged for decreases in porosity (very small changes in the opposite direction account for a change in the specific periphery P_s); 2) the mean grain diameter D increases significantly with decreases in porosity, particularly the gas-flow values, which tend to be a better measure of the internal structure than the metallographic values measured on the surface (the metallographic values are, in turn, more significant in relation to surface properties such as the specific periphery); 3) the permeability decreases with decreases in porosity; and 4) the specific periphery increases slightly, but significantly, with increasing porosity. The increase in D is seen to be accelerated with increasing sintered density, roughly 4, 5, 8, and 19 μ for densities of 60, 70, 80, and 90%, respectively. The permeability, on the other hand, is observed to accelerate with increasing porosity (unity minus the density), very nearly as $k_{20} = 2k_{10}$, $k_{30} = 3k_{10}$, and $k_{40} = 6k_{10}$. There is more than a 25% increase in specific periphery within a given range of surface coverage, between 10 and 40% porosity. Because the forementioned 3) and 4) may be favorable to the attainment of high ion-current density with no apparent reduction in ionization efficiency, a higher ionizer porosity, at any given powder size (pore diameter), is expected to be desirable for ion-propulsion applications.

3. Surface Ionization Apparatus and Techniques

The experimental device used in these studies measured directly and independently the charged and neutral particle fluxes (current densities) extracted and evaporated, respectively, from the porous ionizers. The ion flux was measured by collecting and recording the entire extracted ion current. The neutral flux was determined by selecting and isolating a portion emitted through a known solid angle, ionizing it with a hot tungsten filament, measuring the resulting electron current in this auxiliary ionizer, and calculating the corresponding total emitted neutral flux from knowledge of the geometry and the solid angle, and from the assumption of a cosine distribution of neutral atom emission from the ionizer.

Suppression of all kinds of electron emission from all ion-collecting surfaces was accomplished with highly transparent grids maintained at a negative bias and properly spaced. The suppressed electrons are primarily secondary electrons resulting from ion impact, photoelectrons resulting from the absorption of radiation from the hot ionizer, and thermionic electrons resulting from the heating of the surface because of ion impacts.

A shutter in the neutral particle beam path was employed to ensure accurate measurement of the neutral flux by providing recordings of both the total (shutter open) and background (shutter closed) electron currents in the ionizing filament of the neutral atom detector for each set of experimental conditions. This allows correction for any electron current contributions arising from thermionic emission from the filament, photoelectric emission from the detector body to the filament caused by the absorption of electromagnetic radiation from the hot filament, or ionization in the background vacuum gas in the detector volume. Secondary emission from the filament is negligible because the impinging neutral atoms have only thermal energies.

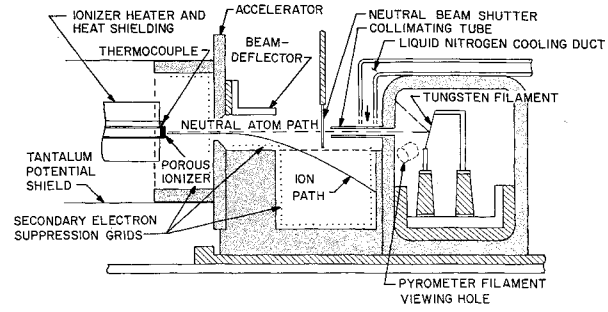

Fig. 3 Schematic of neutral atom detector.

Contrary to the cases of surface ionization by the bulb and the molecular beam methods, the neutral particle current and, hence, the effective neutral flux n_0 reaching the ionizer can be measured for a porous ionizer by electrically shorting the ionizer to the entire surrounding environment (reducing the surface electric field to zero) and measuring the subsequent equilibrium rate of evaporated neutrals which is equal to the flow rate of neutrals through the ionizer. The effective incident neutral flux is then obtained by dividing by the total ionizer area.

The apparatus used for these measurements was located in a vacuum chamber (8 in. in diameter and 24 in. long) in which was maintained a vacuum, during source operation, of from 2×10^{-7} to 3×10^{-6} torr. A particular value depended upon ionizer temperature and beam current, with 1×10^{-6} torr being a normal value. A schematic of the entire system is shown in Fig. 3.

The cesium was stored in a stainless-steel reservoir, the temperature of which could be maintained in the range of 80° to 350°C by a Nichrome heating element embedded in Sauereisen. The reservoir capacity was about 1 g of cesium. A thermocouple was inserted into the body of the reservoir to monitor the temperature of the cesium vapor. To maintain the purity of the cesium at a level as high as possible, the cesium was loaded from 1-g ampoules into the reservoir in an argon atmosphere, after the reservoir and other loading equipment had been in an evacuated chamber adjoining the dry box for several hours. The sealed, loaded reservoir was mounted with the ionizer assembly, as quickly as possible, onto an end plate to minimize leakage of air into the reservoir and was placed in the vacuum system with the neutral-atom detector.

A mechanical valve and a molybdenum delivery tube served as the link between the reservoir and the porous ionizer, which was joined to the end of the delivery tube. The ionizer was heated radiatively by an adjacent tungsten heating element. The ionizer and heating unit were entirely surrounded by many layers of 0.001-in. tantalum heat shielding. The ionizer temperature was monitored by a platinum-platinum (10% rhodium) thermocouple attached at the junction of the ionizer surface and the lip of the delivery tube. Downstream from the ionizer was a large copper structure which served as the accelerating electrode, the beam collector, the neutral beam collimating tube, the housing for the neutral atom detector, and the support for the ion-beam deflector. This entire structure was cooled by liquid nitrogen flow.

The charged portion of the beam, which passed through the hole in the accelerator-collector, was deflected from its initial path into a deep, Faraday collecting cup (Fig. 3) by means of a transverse electrostatic field that was maintained between 0.5 and 0.7 of the accelerating voltage to ensure direction of the entire ion beam into the cup. The beam of neutral particles continued along its original path and passed through a collimating tube 0.125 in. in diameter and 1.5 in. long. The neutral atoms which passed through this collimating tube impinged a tungsten filament, $\frac{3}{4}$ in. long and

0.25 in. wide, which was maintained at a temperature of 1325°K. A hole in the neutral atom detector housing allowed this temperature to be monitored continuously by means of an optical pyrometer, and corrections in the heating current were made as needed to maintain it within the desired degree of accuracy.

The cesium atoms, after being ionized at the hot tungsten surface, were collected by a negative 90 v potential to the main body of the detector. The resulting electron current was measured and used to calculate the ionization efficiency of the ionizer being examined. Typical current ranges were 3×10^{-10} to 5×10^{-9} amp for the background, and 4×10^{-10} to 2×10^{-7} amp for the total current depending upon the ionizer temperature, beam current, and ionization efficiency. Neutral current values were read to three significant figures with an error of about three in the third place.

With this device, it was possible to measure the ionization efficiency and current-voltage characteristics of each porous ionizer as a function of the ion-accelerating potential, the ionizer temperature, the vapor pressure (temperature), and time. For the case of nonporous or filament ionizers, a surface can be largely cleaned of adsorbed foreign atoms by flashing to high temperatures for short periods of time in a high vacuum. For sintered porous ionizers, flashing cannot be safely employed because of the sensitivity of the porous surface structure to high temperatures. Additional sintering (if not rupturing) can occur at temperatures of the order of the original sintering temperature which is sometimes slightly above 2000°C but, in other cases, lower. For example, the 0.9-μ ionizer used in this investigation was sintered and operated up to 1300°C. This is one primary reason why the porous tungsten surface cannot be guaranteed to be free from contamination.

In all of the experiments described herein, a characteristic phenomenon, believed to be the effect of cesium gettering, was consistently observed. This observation led to the establishment of an experimental technique that was employed to obtain all of the data reported. Whenever any ionizer was in a space-charge-limited ion-emitting condition (above the critical temperature threshold and below the saturation electric field), and the ion-extracting electric field was either initially applied or was increased in magnitude, regardless of the initial magnitude, the resulting increase in ion current from the initial value to the final equilibrium value occurred over a time interval of many minutes. When the system was initially started (cesium flow begun), several hours were required for the steady-state current to be attained; after longer periods of operation about 30 min were required. Larger changes in electric field required longer times. Consequently, if it were desirable to plot the ion current as a function of the electric field (current vs voltage) by increasing the electric field in steps, prohibitively long times would have been required to obtain enough points to show the details of the curve, because a wait of many minutes would have been required after each increase of accelerating potential (extracting electric field) to attain the steady equilibrium current. Whenever the magnitude of the electric field was reduced, however, the ion current fell immediately to the equilibrium value corresponding to the new electric field value regardless of the initial value of E. For this reason, all data reported herein were consistently obtained by the following standard operating procedure.

The ionizer temperature and the equilibrium conditions of cesium vapor pressure at the rear of the ionizer were first established at zero electric field. Then the electric field was increased to a maximum value defined by the breakdown threshold of the voltage applied between the ionizer and the accelerating electrode (usually 8 to 10 kv, depending upon the chamber pressure conditions). Thirty minutes to several hours were then required for the ion current to rise to a steady maximum value. The ion and neutral currents were measured at their equilibrium values, corresponding to a series of electric field values always reached by a decrease in applied voltage. Smaller intervals of electric field were used when more detail was desired in the ion-current dependence, for example, at the knee between the emission-limited and the space-charge-limited portions of the curve where an accurate value of the maximum ion current is desired. By acquiring data in this manner, only the long initial wait was required, and much more detailed and accurate information regarding the dependence of the ion current on the applied electric field (voltage) could be obtained during a run time of such duration that variations in thermal equilibrium in the ionizer temperature and the cesium vapor pressure (temperature) could be held to a desirable minimum.

It is possible that, for porous ionizers, the observed slow rises in ion current, which follow successive increases in ion-extracting electric field E but which do not follow similar decreases, are caused by a gradual cleaning of successively larger emitting surface areas around the active pores. Once an equilibrium set of conditions of cesium vapor pressure P_V and ionizer temperature T are established, an emission-limited or saturation current J_+ is defined. When E is zero, no ions can escape ($J_+ \equiv 0$), and because of the pressure drop across the porous ionizer, flow occurs resulting in an equilibrium evaporation rate of neutral cesium from the surface, which has an associated distribution of cesium coverage θ over the surface (θ is large near the active pores and decreases radially outward for a given J_+). For a higher J_+, θ is larger at all points but still decreases radially outward. As an electric field is applied, the corresponding space-charge-limited current is drawn. This current is emitted from the regions of greatest local effective (cesiated) work function ϕ_k which corresponds to the lowest θ_k, i.e., from the areas farthest from the active pores. These areas, therefore, are cleaned of adsorbed cesium, and probably foreign adsorbates, and the regions become even more capable of ion emission because of the increased ϕ_k. As E is increased, the emitting areas expand inward toward the active pores, cleaning larger and larger areas of the surface. The ions are emitted primarily from the peripheries of these clean areas because, although ion emission will occur from any clean (high ϕ_k) area, the areas are fed by neutral cesium only from localized regions (the pores) in the case of porous ionizers. Of course, for filament ionizers, θ and ϕ are essentially uniform (no ϕ_k and θ_k) over the entire surface because cesium is condensing uniformly, and ion sare being emitted relatively uniformly from the surface. Patchy surface effects in ϕ can cause ion emission to be nonuniform on a microscopic scale. As E reaches a value corresponding to the emission-limited current, ion emission occurs nearer the active pores because the cesium is being extracted as ions as fast as it migrates onto the surface. Further increase in E does not necessarily produce more ion current because the current is now limited by the rate of flow of cesium from the active pores.

For the converse case, when the magnitude of E is reduced after equilibrium has been established at the higher value of E, the space-charge-limited current decreases, and the required ion-emitting area decreases. This area has, however, been previously cleaned by the continual ion emission from it, and therefore no gradual cleaning action takes place, and no associated equilibrium time interval is observed. The foregoing arguments are offered only as a possible explanation of the observations, not as proven facts.

4. Surface Ionization Experimental Results

The ionizing surfaces of the porous tungsten ionizers used in this work are very inhomogeneous because of the grain and pore structure in addition to being polycrystalline, and therefore, even more than for solid polycrystalline filament ionizers, are subject to the laws of surface ionization for inhomogeneous or patchy surfaces. The ion-current density emitted from a surface of area A, composed of k types of

patches and from which is emitted a total particle flux n_T, is developed using the following:

$$a_k = (1/C) \exp[(\phi_k + \psi_k - V_i)/kT] \quad (4)$$

$$\beta = \sum_k f_k \beta_k = \sum_k \left[\frac{f_k}{1 + 1/\alpha_k} \right] \quad (5)$$

$$J_+ = e n_T \beta = e n_T \sum_k \frac{f_k}{1 + C \exp[(V_i - \phi_k - \psi_k)/kT]} \quad (6)$$

For solid or filament ionizers, n_T is a function of the vapor pressure only and is independent of T and E. For porous ionizers, n_T is a function of both T and E as well as the vapor pressure. For the regions of the normal and anomalous Schottky effects, the effect of ψ_k is to smooth out the effect of the patchy surface and to make all of the ϕ_k values nearly the same, but not necessarily the average electron work function ϕ_e. The ϕ_k values are functions of θ; ϕ_k decreases with increasing θ_k. For solid ionizers, θ is approximately the same everywhere on the surface, and therefore the ϕ_k values are all reduced by about the same amount. As long as θ is not very large, $2 \exp(V_i - \phi_k - \psi_k)/kT$ will be very much less than unity for the *Cs-W* system and $J_+ \doteq e n_T$. Thus, the patchy theory causes no change in the theory of surface ionization for the *Cs-W* system as long as solid filament ionizers are employed, until θ becomes large enough to cause the ϕ_k values to be reduced to the point where the foregoing inequality does not hold.

For porous ionizers, however, θ may not be uniform over the ionizing surface because of the inhomogeneous pattern of local cesium sources, the pores. The general patchy surface equation can be written as

$$J_+ = e n_T(P_V, T, E) \times \left[\sum_k \frac{f_k}{1 + 2e^{(V_i - \phi_k - \psi_k)/kT}} + \frac{1}{2} \sum_{k'} f_{k'} e^{(\phi_{k'} + \psi_{k'} - V_i)/kT} \right] \quad (7)$$

where k' represents the patches for which $2 \exp(V_i - \phi_k - \psi_k)/kT$ is very much greater than unity (i.e., ϕ_k is large). This is the equation that applies to the cesium-porous tungsten system. Because some terms in the sums increase with T while others decrease, J_+ may be an increasing or decreasing function of T. In addition, because n_T is a function of P_V, T, and E, J_+ may be a complex function of all three variables, and only experiment can determine the relative influences of them. The data obtained in this work indicate that the ion current may increase, decrease, or do both as the ion-extracting electric field is increased. The mode in which a decrease is followed by an increase was most commonly observed.

Data showing the dependence of the cesium ionization efficiency on the initial powder size of the porous tungsten ionizers and on the extracted current density produced by variation of the cesium vapor pressure are shown in Fig. 4. A striking accelerating decrease in the ionization efficiency with increasing powder size is seen. A general decrease in efficiency with increasing ion-current density for all powder sizes is in agreement with a number of other investigations. The curve shown for the 0.9-μ ionizer is drawn from a few points obtained early in its history and at lower current densities. As discussed in a later paragraph, the ionization efficiency of this ionizer actually increased with time; but the cesium transmission decreased severely with operating time. Therefore, a grain size of 0.9 μ appears to be incompatible with high current densities and long operating times. However, if an application requires high ionization efficiency (~99%) for short times at high or low current densities or for long times at low current density, such an ionizer would probably be satisfactory. At no time at current densities of the order of ma/cm^2 can high ionization efficiencies be obtained with powder sizes greater than about 15μ (pore diameters greater than about 8μ). The sharp decrease in efficiency with increasing current density for the larger powder sizes is attributed to increases in the emission of neutral cesium from the large pores as the cesium flow rate increases, changing from the surface migration mode to free molecular flow.

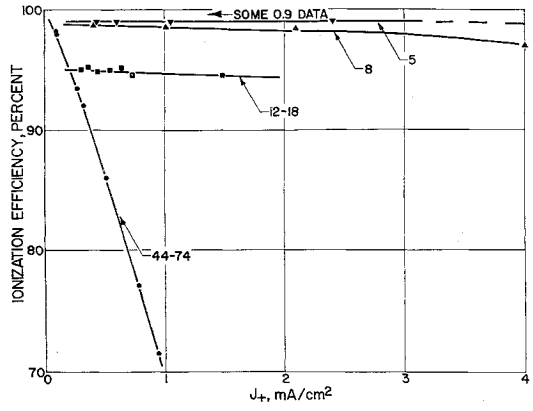

Fig. 4 Ionization efficiency vs ion-current density for various powder sizes.

For an application where high β and high J_+ are simultaneously desirable, and if J_+ is to be increased by increasing P_V at constant T, then these data lead to the conclusion that as small a powder size as possible, within the lower limit imposed by sintering changes (0.9 μ was too small in this work), and as high an ionizer temperature as possible, within the limits imposed by power efficiency (higher T results in higher radiated power losses), are required. The observation that T_c increases with J_+ (discussed elsewhere) is consistent with this desirability of a high T, because T must exceed T_c, but a strong contradiction occurs when the relationship between J_+ and powder size is examined. In that case, the permeability to cesium flow decreases significantly with decreasing ionizer powder size at constant porosity, and, hence, high J_+ and smaller powder size are incompatible. One method for partially correcting for the inhibition of J_+ by small powder size is indicated in Sec. 2 where it is shown that for an 8-μ ionizer the permeability increased with increasing porosity at constant powder size. Thus, high porosity ($\sim\frac{1}{3}$) seems to be valuable in increasing ion-current density with no sacrifice in ionization efficiency, according to the results of this work.

The experimentally measured perveances of the various porous ionizers are shown in Fig. 5. They are seen to increase with increasing current density more rapidly at low values and only slightly at current densities above about 0.5 ma/cm^2.

The curves of Fig. 5 indicate an increase in perveance with a decrease in basic ionizer powder size. An exception is the data for the 0.9-μ ionizer at 1200° C. After the first data were obtained at 1100° C with the 0.9-μ ionizer, the permeability steadily decreased with operating time. Associated increases in densification and number of clogged pores resulted in the sharp decrease in perveance shown in Fig. 5. The data for the 44- to 74-μ ionizer form two curves; one, obtained early in the ionizer's history coincides with those for the other ionizers, and one is much lower. The explanation for the low curve lies in consideration of the ionization efficiency and the fact that the emission-limited ion flux, rather than the total flux, is the ordinate. The "normal" curve was obtained for a low value of vapor pressure where the ionization efficiencies were comparable to those of the other ionizers. The other curve is composed of data obtained at higher values of vapor pressure where the ionization efficiencies were substantially lower than for the other data points, a situation unique to the 44- to 74-μ ionizer.

Any variation of perveance with current density (cesium flux) must be caused by a variation in the effective emitting

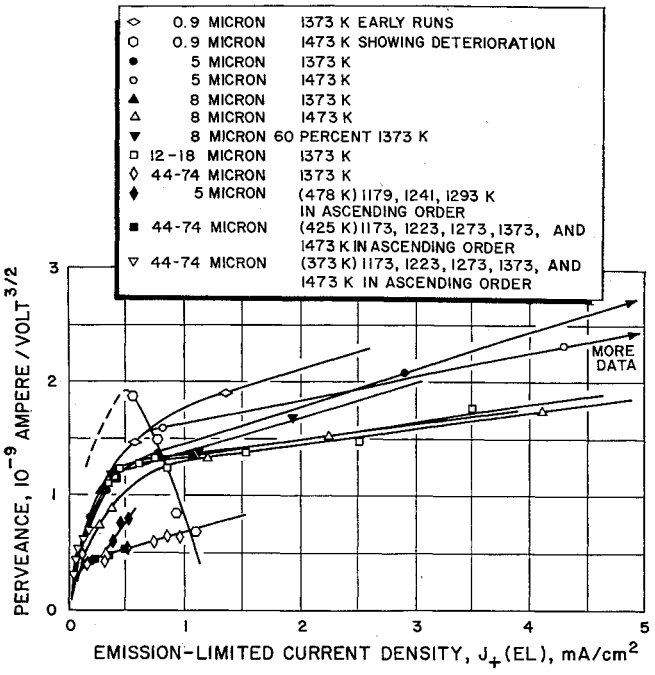

Fig. 5. Perveance of all porous ionizers as a function of ion-current density. The perveances/cm^2 are 3.17 times those shown on the ordinate.

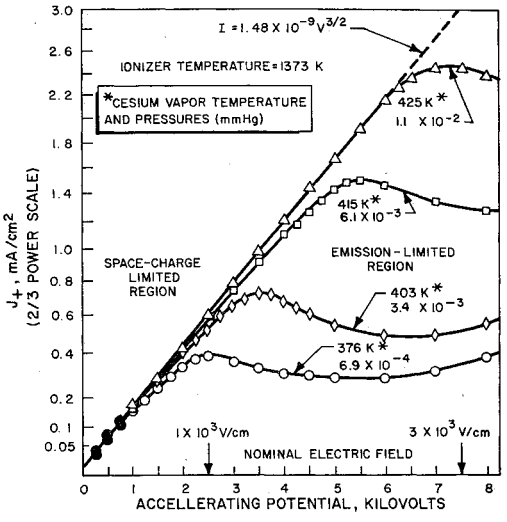

Fig. 6 Current vs voltage characteristic curves as a function of cesium vapor pressure for the 12- to 18-μ powder-size porous tungsten ionizer.

area. That is, as the cesium arrival rate increases, an increasing fraction of the total emitter surface must be ionizing. Two explanations or models can be proposed to account for this effect. First, a sintered porous ionizer is extremely inhomogeneous and patchy in terms of surface structure and work function. A range of patch work functions of approaching one electron volt may occur. At very low cesium arrival rates, the regions with the highest work functions will ionize cesium first and may be of sufficient area to ionize the entire cesium arrival flux. Furthermore, it is known that cesium adsorbs and migrates along particular crystal lattice steps and faces, implying that for low fluxes it will be located only on part of the ionizing surface. As the arrival rate increases, a larger and larger fraction of the surface is required to ionize the entire cesium flux and will be covered with cesium. Gradually, the surface coverage will become large enough on certain patches that the work function will be depressed below other patches of originally lower bare work function. As this situation progresses, the local regions from which ions are emitted change and a progression occurs, until the eventual condition that the coverage becomes sufficiently great to effect a depression in the composite surface work function below the ionization potential and neutral emission increases. This explanation also accounts for a decrease in ionization efficiency with increasing current density because β decreases exponentially as the effective surface work function decreases and, as J_+ increases, ionization occurs on patches with decreasing work function. As the effective emitting area increases, the effective or apparent perveance increases by its definition at low current densities. This argument applies equally well to both porous and polycrystalline ionizing surfaces.

The second concept applies only to porous ionizers. The cesium arrives at the ionizing surface from isolated high concentration sources, the pores, from which it must migrate outward in order to reach the entire surface. For low cesium arrival rates, the surface concentration is low enough even at the pore edges to allow ionization. As the arrival rate to the surface through the pores increases, the surface coverage at pore edges, which must provide the path for cesium to migrate onto the surface, becomes too high to allow ionization (by work function depression), and the ion emitting areas move outward from the pore edges, again changing the regions of ion emission with current density. This concept could explain why the apparent perveance is observed to increase with decreasing pore size and increasing pore density. If this is the explanation, then a correlation might be drawn between the amount of pore edge per unit area and the apparent perveance independent of current density. This accounts for the introduction of the term specific periphery, which is a porous structure term combining the surface density of pores and their diameters by giving a relative measure of the total pore edge per unit area of porous surface.

Values of the specific periphery have been calculated for the ionizers studied and are given in Table 2. The left-hand values of d and S are from the gas-flow measurements, the right-hand values are from the metallographic studies, and the center values are those felt to be the most accurate or are an average and have been used to calculate the quoted values of P_s. It is seen that the 5-, 8-, and 12- to 18-μ ionizers all give nearly the same value, whereas the 44- to 74-μ ionizer yields a value much lower, 0.4 of the former, and the 0.9-μ ionizer shows a much higher value, 3 times the first. Experimentally measured values of the perveance

Table 2 Comparison of calculated specific peripheries and experimental perveances for the porous tungsten ionizers

Basic grain diam, μ	Sintered density, % of theoretical maximum	Mean pore diam d, μ	Mean interpore spacing S, μ	Specific periphery $P_s = 3.6\, d/s^2\, \mu$	Experimental perveance, P^*, 10^{-9} amp/v$^{3/2}$-cm^2 (Pv = 0.06 mm Hg, T = 1100°C)	$P_s \times 79.5$, for comparison to P^*
0.9	76	1.1, 1.1, 1.3	5.4, 5.4, 4.3	0.13	1.90–5.05	10.3
5	80	..., 2.8, 2.8	61, 70, 77	0.070	3.36	5.6
8	68	5.9, 6.0, 6.0	..., 17, 17	0.062	4.85	4.9
12–18	68	16, 13, 9.7	27, 27, 27	0.064	5.08	5.1
44–74	63	35, 37, 40	..., 12, 12	0.027	2.00	2.1

Table 3 History for 0.9-μ ionizer

Run number	T_V, °C	T_V, °C	P_V, mm Hg	History, hr at 1100°C	History, hr at 1200°C	History, hr at 1300°C	$J_0 \times 10^{-15}$ atoms cm^2-sec	$P^* \times 10^9$, amp v$^{3/2}$-cm^2	β_{max}, %
1	1100	196	0.073	3	0	0	2.0	5.7	94½
2	1100	230	0.25	4	0	0	4.0	4.8	94½
3	1200	131	0.0039	4	3	0	1.9	6.0	94¾
4	1200	190	0.057	4	5	0	2.6	4.8	95
5	1200	272	0.97	6	13	0	4.5	2.5	96½
6	1200	270	0.88	9	18	1	2.1	2.2	97½
7	1200	310	2.6	13	19	12	1.6	1.3	98¾

for these five ionizers obtained at $T = 1373$°K and $P_V = 0.06$ mm Hg are also displayed in Table 2 for comparison to the values of the specific periphery.

Apparent perveances for the 8-, 12- to 18-, and 44- to 74-μ ionizers follow quite well the pattern of the specific peripheries, as the normalized values show (Table 2). The values for the 5- and 0.9-μ ionizers are 40 and 50% low, respectively. It is noted, however, that the densities to which these ionizers were sintered are different from those of the larger powder-size ionizers. Those of the 8-, 12- to 18-, and 44- to 74-μ ionizers are very similar, whereas those of the 5- and 0.9-μ ionizers are considerably higher. Because of the higher densities of the latter two, more of the pores that are exposed on the surface may be inactive as a result of internal blocking. Thus, the measured perveance could be expected to be lower than the calculated one. Also, the apparent perveance of the 0.9-μ ionizer decreased with operating time (particularly at high temperatures) as discussed in the next section. This deterioration is attributed to additional sintering implying that pores gradually become closed or clogged internally.

In this study, the experimentally measured values of ion-current density were plotted as a function of applied voltage as shown in Fig. 6, where J_+ is plotted on a $\frac{2}{3}$ powder scale and V on a linear scale. For all the ionizers studied, except the 0.9-μ, plots similar to Fig. 6 were obtained. A series of curves were obtained in each case for different values of cesium vapor pressure at the rear of the ionizer and the corresponding cesium flow rates through the ionizers. As seen in Fig. 6, these curves start out along straight lines, the slopes of which increase slightly but consistently (for all ionizers) with increasing emission-limited ion-current density. For applied voltage above the knee, that is, in the emission-limited current density region, the curves first fall somewhat with increasing applied voltage and then rise at about the same rate as they fell after passing through a minimum, which generally occurred about 3 kv above the knee. There was an indication that this effect increased with increasing grain (and pore) size. Consistent with this last observation was the fact that this effect disappeared for the 0.9-μ ionizer. A curve typical for this ionizer is given in Fig. 7. The space-charge-limited portion of the 0.9-μ ionizer curves was generally more linear with applied voltage, that is, obeyed less closely the perveance relationship, and, in general, did not exhibit the minimum in the curves at higher values of applied voltage (emission-limited region), but rather displayed a continuous increase with voltage. The curves of Fig. 5 show a rise in perveance for low J_+ which occurs within the first $\frac{1}{4}$ ma/cm^2 and which levels out substantially by 0.6 to 0.8 ma/cm^2. The perveance shows a much lower rise with higher magnitudes of J_+.

In the case of the 0.9-μ ionizer, the possibility of changes in the operating characteristics with time at high temperatures existed because the sintering conditions used to obtain the 76% density were only 15 min at 1300°C, and because of the severe changes in porous structure which occurred for the 0.1-μ ionizer at normal ionizer operating temperatures.[3] Operation of this small-grained ionizer at temperatures at and above 1200°C apparently caused additional sintering, resulting in further densification, pore closing, and greater resistance to flow. In Table 3, the ionizer temperature and cesium vapor pressure are shown for a few representative runs, together with an operating history which gives the cumulative hours of operation at 1100°, 1200°, and 1300°C for each of these runs and the measured values of three important operating characteristics: J_0, the neutral cesium flux for no electric field (no ion current); P^*, the apparent perveance, and β_{max}, the maximum ionization efficiency. Because the significance of the J_0 data is difficult to see readily in the form displayed in Table 3, the neutral flux is plotted as a function of the cesium vapor pressure in Fig. 8. The curve formed by data points 1 and 2 (for $T = 1100$°C) is what would be expected from work with other ionizers. These data were obtained before the ionizer had ever been operated at temperatures above 1100°C. Then point 3 was the first one obtained at 1200°C, and a dashed curve is shown, corresponding to what would be expected for a $T = 1200$°C curve. However, points 4 and 5 show that, after several hours of operation at 1200°C, a much larger cesium vapor pressure was required to produce a corresponding neutral flux. Point 6 was obtained at the same vapor pressure and ionizer temperature as point 5, but the ionizer had been subjected to a temperature of 1300°C for one hour, four times the sintering time at the sintering temperature. The neutral flux is seen to have decreased to less than 50% of the former value. Point 7 was obtained after long operation at 1300°C, such that nearly all further sintering effects should have occurred. The neutral flux is down still further even at a 40° higher vapor temperature. The corresponding effects on P^* and β can easily be seen in Table 3. The perveance changed less rapidly at first, but after longer times at 1200 and 1300°C, it dropped sharply, finally, to less than 25% of the original value, implying that the emitting area had decreased and probably that many of the formerly

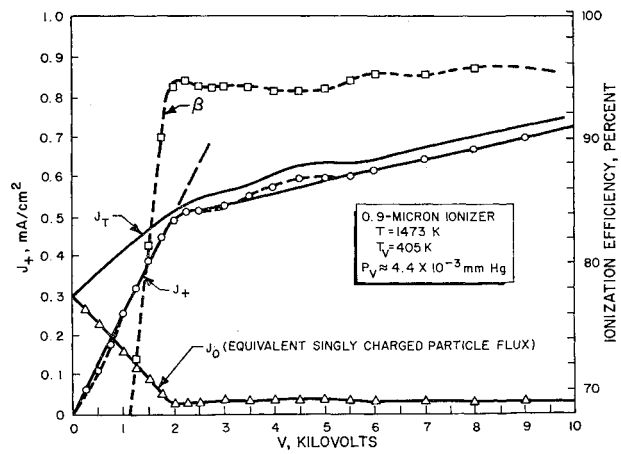

Fig. 7 Current vs voltage characteristics for 0.9-μ ionizer.

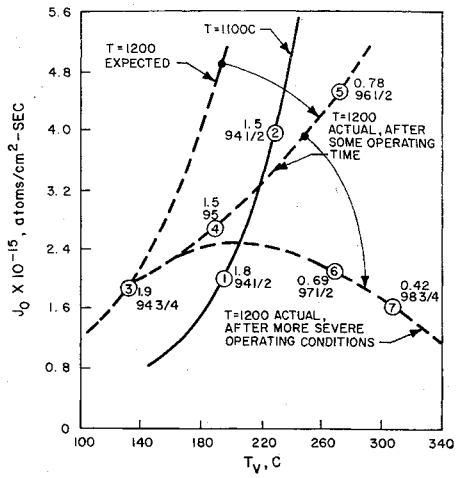

Fig. 8 Effect of operating time at high temperature on flow rate of neutral cesium through 0.9-μ ionizer. Data point numbers represent the run number of Table 3 in which the operating history is given. The first number by the data point is the perveance ($\times 10^9$), and the second number is the ionization efficiency.

active pores had closed or become blocked. The emission-limited ionization efficiency increased only slowly at first, but by the final run (No. 7) had increased to a value corresponding to a reduction in the neutral fraction of more than 75%, probably indicating a general shrinkage in pore size (diameter).

The critical temperature for surface ionization is here defined as the temperature at which the break occurs in the saturated ion-current density vs temperature curve. According to the data presented in this work, it is not necessarily the temperature at which the maximum ion-current density can be drawn, nor the ionizer temperature at which the maximum ionization efficiency occurs. The most reliable data obtained in this work for the variation of T_c with J_+ are plotted in Fig. 9, together with some other published data for the ionization of cesium on porous tungsten[6-8] and one curve for cesium and filament tungsten for comparison.[17] The values of T_c reported here were obtained from curves of the maximum emission-limited ion-current density vs ionizer temperature obtained in turn, from plots of J_+ vs E at many various T's, not from a single plot of J_+ vs T at one particular value of V (or E). This explains in part why the experimental data for porous ionizers exhibit such a degree of scatter and why they do not all agree with the solid tungsten curve, which was obtained at a constant high value of applied electric field, 1.3×10^4 V/cm.[18] The electric field dependence of the critical temperature is seen in the expression

$$J_+ = \frac{e\theta_c\sigma(1)}{2}\left(\frac{kT_c}{h}\right)\left[1 - e^{-(hw/kT_c)}\right]^{-1} \times \exp\left[-\frac{\lambda_+(\theta_c) - e(eE)^{1/2}}{kT_c}\right] \quad (8)$$

for $E \leq 10^6$ V/cm.

It was observed in this work that, if T_c was obtained from simple plots of J_+ vs T at some arbitrary constant value of E, the points for T_c vs J_+ fell toward higher temperatures and with more scatter.

One other possible cause of the data scatter could be varying degrees of surface contamination. Foreign atoms chemisorbed on the surface could cause the effective critical temperature to be raised[18] because the work functions of the surface patches would be lowered by most foreign adsorbates.

In Ref. 7, it was observed that for a porous tungsten ionizer the maximum β occurred about 100°K above T_c. In this work it is observed that β_{max} occurs at a T above T_c, but that the amount varies inversely with β_{max}. When the maximum emission-limited current is plotted as a function of T, β_{max} occurs within about 20°K when β_{max} is 98 to 99%, within about 50°K when β_{max} is about 95%, within 120°K when β_{max} is approximately 90%, and as much as 250°K higher when β_{max} is as low as 70%. If β is plotted as a function of T for various V (or E), as in Fig. 10, the variation of β with E is illustrated and it is seen that, for certain V, β_{max} may occur for a T closer to T_c.

One measurement of the surface ionization critical temperature hystersis for a porous tungsten ionizer was made. This hysteresis is defined as the difference in the critical temperature at which saturation of the ion-current density exists for increasing or decreasing surface temperature in the critical region. For the 5-μ porous ionizers, at a cesium ion flux of 2.5×10^{15}/cm^2-sec, essentially no difference ($\lesssim 5K$) was observed between the critical temperatures for increasing or decreasing temperature for a measurement made very carefully and slowly (over a period of several hours). Critical temperature hysteresis effects have been reported for solid polycrystalline tungsten and rhenium ionizers by Taylor[19] and other authors. This effect is currently being studied in detail by Robert Wilson[18,20] for a number of polycrystalline metal surfaces by a new technique that allows the influence of time, as well as the usual variables, on the effect to be determined. It has been found that the effect is time-dependent. The results of these measurements also show reproducible fine structure in the current density vs temperature plots in the critical region.

In Ref. 21 the various modes for the passage of gases through porous media are considered in detail. The validity of the basic assumptions underlying their application to the case of alkali metals and refractory metal porous ionizers is examined. Comparable equations governing flow through porous ionizers are developed. Consideration of the basic assumptions for the equations and the dependence on pressure, temperature, and porous structure, compared with experimental results, indicates that the transport occurs primarily as simple surface migration or diffusion at lower flow rates with free molecular flow contributing an increasing fraction of the total flow as the flow rate increases, probably accounting in some degree for the observed decrease in surface ionization efficiency with increasing flow rate because of the increase in arriving neutral atoms not in contact with the ionizing surface. Other modes, such as viscous flow,

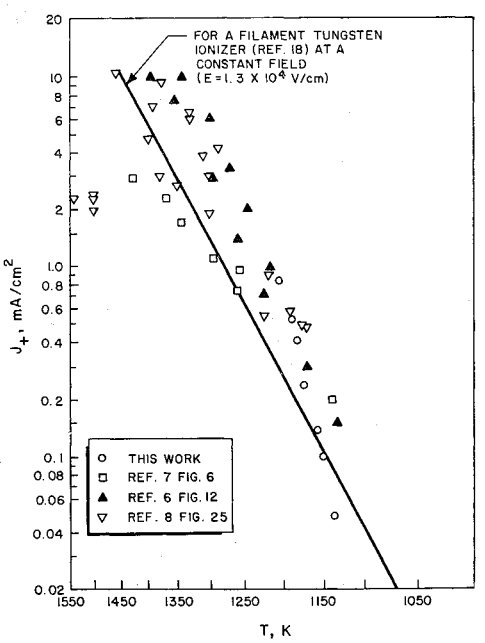

Fig. 9 Critical temperatures as a function of current density for porous tungsten ionizers.

and flow by capillary condensation are, at most, secondary modes of transport in the pressure range of interest. Viscous flow is ruled out relative to free molecular flow because the magnitude of λ/D, the ratio of the mean free path of the transport molecule to the pore diameter, is 10^3 to 10^6. For the case of cesium flow through porous tungsten, the three remaining modes must be considered and compared to the experimental results.

The equations developed for the three modes are shown below written in comparable form with four groups of terms: constants, porous structure parameters, pressure, and temperature. For free molecule flow,

$$n_0 = \frac{1}{3}\left(\frac{\pi N_a}{2kM}\right)^{1/2}\left\{\frac{Hd^3}{L_c}\right\}\{P_V\}\{T^{-1/2}\} \tag{9}$$

For surface migration (or diffusion) (monolayer or less),

$$n_0 = \frac{\alpha}{4}\left(\frac{N_a}{kM}\right)^{1/2}\left\{\frac{\delta P_s}{S_v L_c}\right\}\left\{\left(\frac{L_c}{L}\right)^2\right\}\{P_V\}\{T^{-1/2}e^{-V_m/kT}\} \tag{10}$$

For capillary condensation,

$$n_0 = \frac{\pi N_a^2}{4M^2}\left\{\frac{Hd^2k_p}{L_c}\right\}\left\{\ln\left(\frac{P_V}{P_0}\right)\right\}\left\{\frac{T\rho_c^2(T)}{\eta_c(T)}\right\} \tag{11}$$

The derivation of the free molecule mode requires the assumption of the existence of adsorption of the transport molecules for a certain length of time following collisions with the porous medium channel walls. Provided that the volume of the adsorbed surface diffusion film comprises a negligible part of the total pore volume, it should exert no influence on the steady-state flow of the gaseous phase, whether viscous or free molecule.[22] Therefore, simultaneous transport by both free molecular flow and surface diffusion can occur. While N_2, H_2, and the inert gases have been described as relatively nonsorbably (physisorption), the alkali metals are very sorbably (combination of ionic and covalent bonding[23]). Oxygen and carbon are two elements which are also strongly chemisorbed on tungsten and may be present in these experiments as contaminants. They are bound to the tungsten surface by much higher energies (heats of adsorption) and hence are much more difficult to remove. They migrate

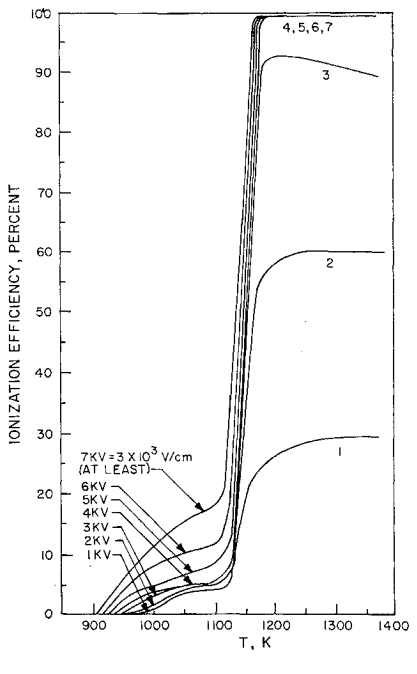

Fig. 10 Ionization efficiency vs temperature at various voltages (5-μ ionizer).

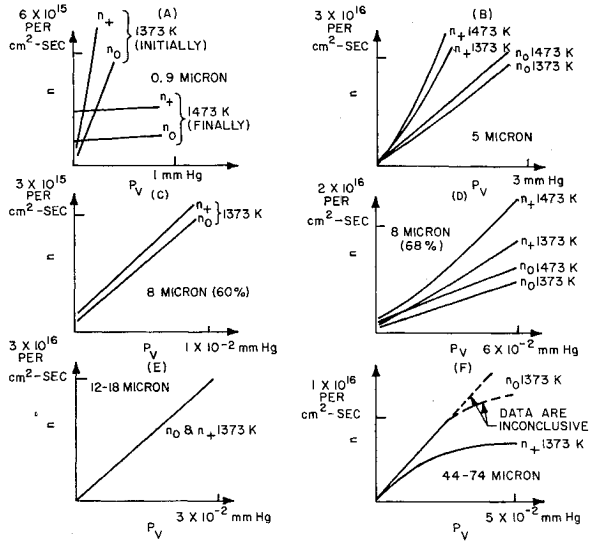

Fig. 11 Particle fluxes vs cesium vapor pressure relationships. The values of n_0 are for no electric field and hence no ion emission.

according to different laws and, in time, can penetrate into the tungsten structure. These two elements cannot be completely removed by high-temperature flashing of tungsten surfaces. Any oxygen or carbon impurities existing in the porous tungsten, incident from the ambient vacuum environment, or in the diffusing cesium will become chemisorbed in the tungsten ionizer over the period of operation. Oxygen may have a favorable effect because it increases the work function of the ionizing surface, but it also increases the critical temperature for ion production. Carbon is expected to lower significantly the surface work function at low coverages while also increasing the cesium ion-critical temperature.[18] Over a long operation time, carbon might tend to clog narrow flow channels by the build-up of tungsten carbides (chemisorbed carbon).

Three primary factors influence the cesium flow through the ionizer and, hence, the rate of delivery of the cesium to the front ionizer surface. These factors are: 1) the cesium vapor pressure at the rear ionizer surface, 2) the ionizer (porous plug) permeability, and 3) the ionizer temperature. For filament ionizers, only the vapor pressure (or beam flux) determines the total particle flux (ions plus neutrals) that can leave the ionizer surface; this quantity is independent of the ionizer temperature, and no permeability concept exists. The influence of the vapor pressure at the rear of a porous ionizer is two-fold. It determines the flux of incident adatoms onto the rear surface, and it produces the pressure drop across the porous plug. The porous ionizer structure determines its permeability. At constant ionizer temperature the vapor pressure and permeability should determine the flow rate through the ionizer. The data that illustrates this relationship are shown in Fig. 11 for all of the ionizers studied, and Fig. 12 is one representative case showing the actual data points. In every case, data for an ionizer temperature of 1373°K are included, and in some cases, data are also shown for 1473°K. The curves of n_0 (neutral particle flux) are for no electric field and consequently no ion emission. In all cases, linear relationship is exhibited between n_0, and P_V is the only variable influencing flow. This is consistent with either surface diffusion or the free molecular (Knudsen) flow regime, in each of which the flow rate is proportional to the pressure drop and is not consistent with flow by capillary condensation [Eqs. (9–11)]. The slopes of the curves of n_0 vs P_V ($E = 0$) for the various ionizers are displayed in Table 4 together with the ionizer permeabilities from the gas flow measurements. The slopes are $\Delta n_0/\Delta P_V$

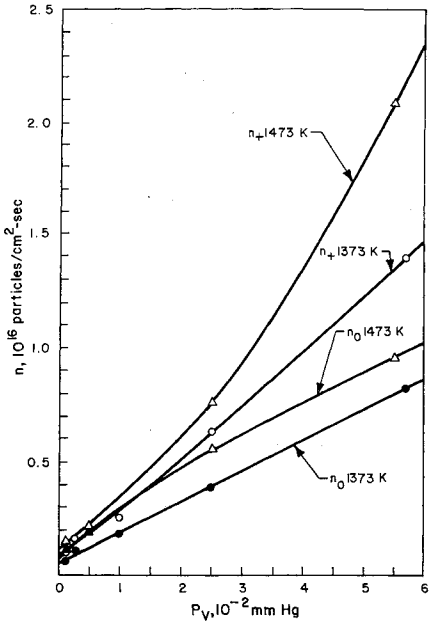

Fig. 12 Particle fluxes vs cesium vapor pressure for 8-μ (68% dense) ionizer.

in atoms/cm²-sec mm Hg. A favorable comparison is observed in all cases except for the largest powder size.

The data for the 0.9-μ ionizer show the effect of operating time. The steep curves (at 1373°K) were taken early in the ionizer's history and can be used to compare with the other ionizers for powder-size effects. The nearly flat curves (at 1473°K) were obtained at approximately the time that the permeability measurement reported in Table 1 was made and should therefore be used in comparison with the measured permeability.

For all of the porous tungsten ionizers and the conditions of this work (cesium ion-current densities in the range 10^{-3} to 1 ma/cm²), the flow of neutral cesium through the ionizers, as measured directly by the neutral atom detector in the absence of any ion emission (zero electric field), was observed to increase with ionizer temperature when all other variables were held constant. As already discussed, the cesium flow is expected to be a combination of surface diffusion and free molecule flow. The total flow rate (or particle flux) would thus be the sum of a term proportional to $T^{-1/2}$ (free molecule) and a term proportional to $T^{-1/2}\exp(-V_m/kT)$, a modified exponential that, at large T and over a small range of T, could appear to increase nearly linearly with T. This dependence would exhibit an extrapolated positive temperature intercept if the exponential term predominated. The

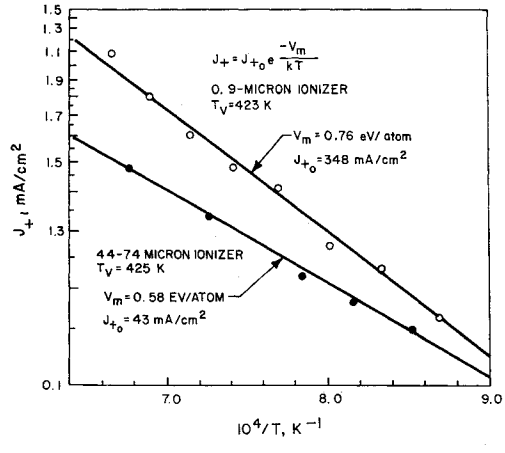

Fig. 13 Data illustrating relationship of Eq. (12).

Table 4 Comparison of ionizer permeability and slope of particle flux vs P_V at 1373°K ionizer temperature

Powder size, μ	Density, %	Permeability, cm²	Slope, particles/cm²-sec-mm Hg
0.9	76	?$\rightarrow 9\times10^{-12}$	$4\times10^{15}\rightarrow 2\times10^{14}$
5	80	$\sim 3\times10^{-10}$	1.2×10^{16}
8	68	$\sim 2\times10^{-9}$	1.4×10^{17}
8	60	$\sim 7\times10^{-9}$	2.6×10^{17}
12–18	68	2×10^{-8}	8×10^{17}
44–74	63	9×10^{-8}	5×10^{17}

relative magnitude of V_m compared to kT determines the relative strength of the exponential; if V_m/kT is large, the exponential will predominate. The curves of $n_0(T)$ exhibit a stronger exponential dependence at lower flow rates possibly indicating an increase of free molecule flow at higher flow rates. Consistent with this premise and with the combination of surface diffusion and free molecule flow modes are the results of experiments of Kuskevics and Thompson[11] at higher cesium ion-current densities. Using the same experimental techniques and similar porous ionizers, but at current densities one to three orders of magnitude larger, they observed a decrease in current density with temperature, stronger at 12 ma/cm² than at 8 ma/cm² where it is only slightly temperature-dependent. The results of these two investigations indicate that the transition from predominant surface diffusion to predominant free molecule flow occurs in the range from 0.5 to 5 ma/cm². The curves of emission-limited ion-current density $\leq$ 1 ma/cm² obtained from this investigation fit the expected exponential form

$$J_+ = J_{+0}\, e^{-V_m/kT} \qquad (12)$$

Table 5 is a tabulation of the values of V_m and J_{+0} together with the average ionization efficiencies obtained from plots of $\ln J_+$ vs $1/T$ for the cases that gave the best straight lines with a minimum of five data points. Two examples are illustrated by Fig. 13. The two lowest values of V_m in Table 5, 0.59 ev/atom, are the value found in the literature for the energy of surface migration of cesium on solid tungsten measured by other techniques. The average of all of the experimentally measured values of V_m for porous tungsten, 0.68 ev/atom, is slightly higher.

The ratio of the total particle flux for emission-limited ion production (high electric field) to total neutral flux (E = 0) was observed to decrease consistently with powder size for the five sizes investigated. The maximum value was observed to be about 2, for the small powder sizes are the minimum, about $\frac{1}{2}$, for the largest size. The 12- to 18-μ size exhibited a value of unity for this ratio.

The largest powder-size ionizer was fabricated from particle diameters in the range 44 to 74 μ. The resulting mean pore diameter was about 37 μ. This specimen yielded some experimental results which differed from those of the smaller powder-sized ionizers, characterized by low ionization efficiencies and sharp decreases in ion-current density with increasing ionizer temperature.[21] Some of the differences can certainly be attributed to the large pore diameter. The

Table 5 Experimental values of constants in Eq. (7)

Powder size, μ	T_V, K	J_{+0}, ma/cm²	V_{m+}, ev/atom	β, %
0.9	423	348	0.76	95½
0.9	463	180	0.59	95½
8	443	150	0.77	95
12–18	388	273	0.72	95
44–74	425	43	0.59	90
Averages		200	0.68	

results indicate that such an ionizer is not suitable for a high efficiency device.

References

[1] Stavisskii, Yu. Ya. and Lebedev, S. Ya., "Surface ionization of cesium upon diffusion through porous tungsten," Soviet Tech. Phys. **5**, 1158–1161 (1960).

[2] Langmuir, D., Stuhlinger, E., and Sellen, J. (eds.), *ARS Progress in Astronautics and Rocketry: Electrostatic Propulsion* (Academic Press, Inc., New York, 1961).

[3] Hubach, R. A. and Seele, G. D., "Properties of porous tungsten and ionization of cesium," ARS Paper 1780 (1961); also Air Force Systems Command, Aeronautical Systems Div. TR 61-320 (1961).

[4] Reynolds, T. W. and Kreps, L. W., "Gas flow, emittance and ion current capabilities of porous tungsten," NASA TN D-871 (1961).

[5] Dalins, I., "Flow through porous media and its implications for ion rocket operation," ARS Paper 2362 (1962).

[6] Husmann, O. K., "Experimental evaluation of porous materials for surface ionization of cesium and potassium," ARS Paper 2359 (1962).

[7] Shelton, H., "Experiments on atom and ion emission from porous tungsten," ARS Paper 2360 (1962); also "Surface diffusion studies of cesium on tungsten," ARS J. **32**, 708 (1962).

[8] Taylor, L. H. and Todd, H. H., "Ionizer development and surface physics studies," NASA Contract Interim Summary Rept. NAS 8-1537 (1962).

[9] Shelton, H. and Cho, A., "Program of analytical and experimental study of porous metal ionizers," NASA Contract Rept. NAS 3-5254 (1964–1965).

[10] Husmann, O. K., "A comparison of the contact ionization of cesium on tungsten with that of molybdenum, tantalum, and rhenium surfaces," AIAA Preprint 63-019 (1963); also AIAA J. **1**, 2607–2614 (1963).

[11] Kuskevics, G. and Thompson, B. L., "Comparison of commercial, spherical powder, and wire bundle tungsten ionizers," AIAA Preprint 63-016 (1963); also AIAA J. **2**, 284–294 (1964).

[12] Marchant, A. B., Kuskevics, G., and Forrester, A. T., "Surface ionization microscope," AIAA Preprint 63-018 (1963).

[13] Shelton, H., "Research and development of porous tungsten ion emitters for use in electrostatic propulsion," NASA Contract Summary Rept. NAS 8-41 (1963).

[14] Adzumi, H., "Flow of gases through a porous wall," Bull. Chem. Soc. Japan **12**, 304 (1937).

[15] Deryagin, B. V., "Determination of the specific surface of powders used in the production of hard alloys," Tsvethyye Metally **11**, 55 (1959).

[16] Kraus, G., Ross, J. W., and Girifalco, L. A., "Surface area analysis by means of gas flow methods," J. Phys. Chem. **57**, 330–333 (1953).

[17] Zandberg, E. Ya., Paleev, V. I., and Tontegode, A, Ya., "Threshold temperature for surface ionization on tungsten as a function of the cesium vapor pressure," Soviet Tech. Phys. **7**, 147–151 (1962).

[18] Wilson, R. G., "Electrode Surface Physics Research," NASA Progress and Final Repts., Contract NAS 3-5249 (1964); also Wilson, R. G., "Thrustor Electrode Surface Physics Studies," NASA Progress and Final Repts., Contract NAS 3-6278 (1965).

[19] Taylor L. H., "Adsorption of cesium on polycrystalline refractory metals," *1964 International Conference on Physics and Chemistry of Solid Surfaces* (North-Holland Publishing Co., Amsterdam, Holland, 1964), pp. 188–199.

[20] Wilson, R. G., "Electrode surface physics research," NASA Quarterly Progress Rept. 2, Contract NAS 3-5249 (October 1964).

[21] Wilson, R. G., Seele, G. D., and Hon, J. F., "Surface ionization of cesium with porous tungsten ionizers," AIAA Preprint 63-017 (1963).

[22] Carman, P. C., *Flow of Gases Through Porous Media* (Butterworth Scientific Publications Ltd., London, 1956, and Academic Press, Inc., New York, 1956).

[23] Levine, J. D. and Gyftopoulos, E. P., "Adsorption physics of metallic surfaces partially covered by metallic particles—I. Atom and ion desorption energies," Surface Sci. **1**, 171–193 (1964).